

# PARAMETRIC FREQUENCY ANALYSIS OF MATHIEU-DUFFING EQUATION

MOHSEN AZIMI \*

*Department of Aerospace and Mechanical Engineering, University of Arizona  
Tucson, Arizona 85721, US*

Received (to be inserted by publisher)

The classic linear Mathieu equation is one of the archetypical differential equations which has been studied frequently by employing different analytical and numerical methods. The Mathieu equation with cubic nonlinear term, also known as Mathieu-Duffing equation, is one of the many extensions of the classic Mathieu equation. Nonlinear characteristics of such equation have been investigated in many papers. Specifically, the method of multiple scale has been used to demonstrate the pitchfork bifurcation associated with stability change around the first unstable tongue and Lie transform has been used to demonstrate the subharmonic bifurcation for relatively small values of the undamped natural frequency. In these works, the resulting bifurcation diagram is represented in the parameter space of the undamped natural frequency where a constant value is allocated to the parametric frequency. Alternatively, this paper demonstrates how the Poincare-Lindstedt method can be used to formulate pitchfork bifurcation around the first unstable tongue. Further, it is shown how higher order terms can be included in the perturbation analysis to formulate pitchfork bifurcation around the second tongue, and also subharmonic bifurcations for relatively high values of parametric frequency. This approach enables us to demonstrate the resulting global bifurcation diagram in the parameter space of parametric frequency, which is beneficial in the bifurcation analysis of systems with constant undamped natural frequency, when the frequency of the parametric force can vary. At the end, the analytical approximations are verified by the employment of the numerical integration along with Poincare map and phase portray.

*Keywords:* Pitchfork bifurcation; Subharmonic bifurcation; Parametric frequency analysis; Cubic nonlinear term

## 1. Introduction

The classic linear Mathieu equation is a special case of the Hill equation [Rodriguez & Collado, 2015] and various analytical techniques including: Strained Parameter method, Averaging Method [Shivamoggi, 2003], Harmonic Balance method, Method of Multiple Scale [Kovacic *et al.*, 2018], and numerical approaches including: Floquet Theory [Kovacic *et al.*, 2018] and Energy Rate Method [Jazar *et al.*, 2008] have been used to study the stability of this equation. Consequently, various extensions of the classical Mathieu equation with additional terms like linear viscous damping [Acar & Feeny, 2016], geometric or damping nonlinearities [Ng & Rand, 2002], delay [Morrison & Rand, 2007], fractional derivative [Leung

---

\*E-mail: azimimohsen@email.arizona.edu

*et al.*, 2012], higher order derivatives [Subhadip & K., 2019], coupling [Welte *et al.*, 2013], quasiperiodic excitation [Rand & Morrison, 2005], elliptic excitation [Kovacic *et al.*, 2018], and harmonic excitation [Rodriguez & Collado, 2015; Ramakrishnan & Feeny, 2012] have been thoroughly considered as they arise in mathematical modeling of various dynamic systems. Specifically, there have been many analytical and numerical investigations on the characteristics of the Mathieu-Duffing equation. It has been shown that under influence of cubic nonlinearity and with different combinations of the parameters, the number of the equilibrium points and stability of the origin can change. The method of multiple scale has been used to demonstrate the pitchfork bifurcations around the first unstable tongue [Kovacic *et al.*, 2018] and Lie transform has been used to demonstrate the subharmonic bifurcations for small values of natural frequency [Zounes & Rand, 2002], which all have been represented in the parameter space of the undamped natural frequency, where a constant value is allocated to the parametric frequency.

Alternatively, in this work, the Poincare-Lindstedt method is used to obtain the bifurcation diagram around the first unstable tongue. Moreover, it is shown how higher order terms in the perturbation analysis can be included to demonstrate occurrence of the pitchfork bifurcation around the second unstable tongue and subharmonic bifurcation for relatively high values of parametric frequency. Employment of the Poincare-Lindstedt method enables us to demonstrate the global bifurcation diagram of the Mathieu-Duffing equation in the parameter space of the parametric frequency [Acar & Feeny, 2016], which is more beneficial in frequency analysis of systems with constant undamped natural frequency, when the frequency of the parametric force can change. In this work, all the analytical equations are provided as a function of undamped natural frequency, unlike previous works that expressed the results only for a specific value of natural or parametric frequencies [Cveticanin & Kovacic, 2007]. Numerical integrations are carried out along with the Poincare map and phase portray to validate the accuracy of the analytical calculations.

The rest of this paper is organized as follows: In section 2, analytical calculation is used to demonstrate the creation and stability of new equilibrium points; in section 3, the results of the numerical calculations are provided to validate the analytical results. At the end, the conclusion and remarks are presented.

## 2. Analytical Calculations

In this section, Poincare-Lindstedt method is used to study the change of the stability around the first unstable tongue, second unstable tongue, and for relatively large values of parametric frequencies, respectively. The unperturbed Mathieu equation with cubic nonlinear term is written in the following standard form.

$$\ddot{x} + \zeta \dot{x} + (\omega_n^2 + F_p \cos \omega_p t)x + \alpha x^3 = 0 \quad (1)$$

Where the constant parameters  $\zeta, \omega_n, \omega_p, F_p$  and  $\alpha$  are the damping ratio, undamped natural frequency, parametric frequency, parametric amplitude, and nonlinear stiffness, respectively. By introducing the small parameter  $\epsilon$  to perturb the time varying and nonlinear terms and using the following time scale

$$\tau = \omega_p t, \quad \ddot{x} = \omega_p^2 x'' \quad (2)$$

one can find the corresponding undamped perturbed form of (1).

$$\omega_p^2 x'' + (\omega_n^2 + \epsilon \cos \tau)x + \epsilon \alpha x^3 = 0 \quad (3)$$

where prime represents derivation with respect to the new variable  $\tau$ . By expanding  $x$  and  $\omega_p$  into power series,

$$x = x_0 + x_1 \epsilon + x_2 \epsilon^2 + x_3 \epsilon^3 + \dots \quad (4)$$

$$\omega_p = \omega_0 + \omega_1 \epsilon + \omega_2 \epsilon^2 + \omega_3 \epsilon^3 + \dots \quad (5)$$

substituting (4) and (5) in (3), dropping terms of  $O(\epsilon^3)$ , and collecting terms of the same power, the following equations are obtained.

$$x_0'' + \left(\frac{\omega_n}{\omega_0}\right)^2 x_0 = 0 \quad (6)$$

$$x_1'' + \left(\frac{\omega_n}{\omega_0}\right)^2 x_1 = -2\left(\frac{\omega_1}{\omega_0}\right)x_0'' - \left(\frac{1}{\omega_0}\right)^2 x_0 \cos\tau - \frac{\alpha}{\omega_0^2} x_0^3 \quad (7)$$

$$x_2'' + \left(\frac{\omega_n}{\omega_0}\right)^2 x_2 = -\left[\left(\frac{\omega_1}{\omega_0}\right)^2 + 2\left(\frac{\omega_2}{\omega_0}\right)\right]x_0'' - 2\left(\frac{\omega_1}{\omega_0}\right)x_1'' - \left(\frac{1}{\omega_0}\right)^2 x_1 \cos\tau - \frac{3\alpha}{\omega_0^2} 2x_0^2 x_1 \quad (8)$$

Equation (6) is a simple harmonic oscillator, with the following general solution.

$$x_0(\tau) = A \cos \frac{\omega_n}{\omega_0} \tau + B \sin \frac{\omega_n}{\omega_0} \tau \quad (9)$$

Substituting (9) in (7), simplifying the trig functions, and collecting terms with the same frequency results in

$$\begin{aligned} x_1'' + \left(\frac{\omega_n}{\omega_0}\right)^2 x_1 = & \\ & + \left[-\frac{3\alpha}{4\omega_0^2}(A^2 + B^2) + 2\left(\frac{\omega_1}{\omega_0}\right)\left(\frac{\omega_n}{\omega_0}\right)^2\right]A \cos \frac{\omega_n}{\omega_0} \tau \\ & - \left[+\frac{3\alpha}{4\omega_0^2}(A^2 + B^2) - 2\left(\frac{\omega_1}{\omega_0}\right)\left(\frac{\omega_n}{\omega_0}\right)^2\right]B \sin \frac{\omega_n}{\omega_0} \tau \\ & - \frac{1}{2\omega_0^2} \left[A \cos\left(\frac{\omega_n}{\omega_0} - 1\right)\tau + B \sin\left(\frac{\omega_n}{\omega_0} - 1\right)\tau\right] \\ & - \frac{1}{2\omega_0^2} \left[A \cos\left(\frac{\omega_n}{\omega_0} + 1\right)\tau + B \sin\left(\frac{\omega_n}{\omega_0} + 1\right)\tau\right] \\ & - \frac{\alpha}{4\omega_0^2} \left[(A^2 - 3B^2)A \cos \frac{3\omega_n}{\omega_0} \tau + (3A^2 - B^2)B \sin \frac{3\omega_n}{\omega_0} \tau\right] \end{aligned} \quad (10)$$

which contains harmonic functions with frequencies equal to

$$\frac{\omega_n}{\omega_0}, \frac{3\omega_n}{\omega_0}, \frac{\omega_n}{\omega_0} \pm 1 \quad (11)$$

### 2.1. Bifurcation Around the First Tongue

The emanating frequency of the first tongue in the Ince-Strutt stability diagram is corresponded to the following special condition [Nayfeh & Mook, 1995].

$$\left(\frac{\omega_n}{\omega_0}\right) - 1 = -\left(\frac{\omega_n}{\omega_0}\right) \rightarrow \omega_0 = 2\omega_n \quad (12)$$

In such a case the first three terms on the right-hand side of (10) are the resonance terms and the following conditions are required to remove the secular terms.

$$\left[+\frac{3\alpha}{16\omega_n^2}(A^2 + B^2) - \frac{1}{4}\left(\frac{\omega_1}{\omega_n}\right) - \frac{1}{8\omega_n^2}\right]B = 0 \quad (13)$$

$$\left[-\frac{3\alpha}{16\omega_n^2}(A^2 + B^2) + \frac{1}{4}\left(\frac{\omega_1}{\omega_n}\right) - \frac{1}{8\omega_n^2}\right]A = 0 \quad (14)$$

Removal of the resonant terms when  $\alpha = 0$  provides the first order multipliers of the first tongue's transition curves.

$$\omega_1 = -\frac{1}{2\omega_n}, +\frac{1}{2\omega_n} \quad (15)$$

By defining the polar coordinates,  $A = R\cos\theta$  and  $B = R\sin\theta$ , the alternate polar form of (13) and (14) are obtained.

$$\left[ +\frac{3\alpha}{16\omega_n^2}R^2 - \frac{1}{4}\left(\frac{\omega_1}{\omega_n}\right) - \frac{1}{8\omega_n^2} \right] R\sin\theta = 0 \quad (16)$$

$$\left[ -\frac{3\alpha}{16\omega_n^2}R^2 + \frac{1}{4}\left(\frac{\omega_1}{\omega_n}\right) - \frac{1}{8\omega_n^2} \right] R\cos\theta = 0 \quad (17)$$

Solving (16) and (17) results in the following five equilibrium points.

$$R_1 = 0 \quad (18)$$

$$R_{2,3}^2 = \frac{2}{3\alpha}(2\omega_n\omega_1 + 1) \quad \theta = \frac{\pi}{2}, \frac{3\pi}{2} \quad (19)$$

$$R_{4,5}^2 = \frac{2}{3\alpha}(2\omega_n\omega_1 - 1) \quad \theta = 0, \pi \quad (20)$$

Such that  $R_1$  is corresponded to the trivial equilibria at origin and each of  $R_{2,3}$  and  $R_{4,5}$  is corresponded to two nontrivial equilibria located  $\pi$  (*rad*) apart from each other. The creation and local stability of these equilibrium points is determined by the eigenvalues of the Jacobian matrix corresponded to (13) and (14).

$$J = \begin{bmatrix} \frac{3\alpha}{16\omega_n^2}(2AB) \\ \frac{3\alpha}{16\omega_n^2}(A^2 + 3B^2) - \left(\frac{\omega_1}{4\omega_n} + \frac{1}{8\omega_n^2}\right) \\ -\frac{3\alpha}{16\omega_n^2}(3A^2 + B^2) + \left(\frac{\omega_1}{4\omega_n} - \frac{1}{8\omega_n^2}\right) \\ -\frac{3\alpha}{16\omega_n^2}(2AB) \end{bmatrix} \quad (21)$$

Alternatively, for a  $2 \times 2$  matrix the Trace (*Tr*) and Determinant (*Det*) of the Jacobian matrix can be used to form the characteristic equation.

$$\lambda^2 - Tr(J)\lambda + Det(J) = 0 \quad (22)$$

For (21), the *Tr* is always equal to zero and the value of the *Det* is expressed by the following equation.

$$Det(J) = \frac{27\alpha^2}{4}(A^2 + B^2)^2 - 12\alpha\omega_n\omega_1(A^2 + B^2) - 3\alpha(A^2 - B^2) + (4\omega_n^2\omega_1^2 - 1) \quad (23)$$

Since the value of *Tr* is always equal to zero, the eigenvalues of the Jacobian matrix have the same magnitude with opposite signs, for every  $\omega_1$ . Such that for the positive values of the *Det* both eigenvalues are on the imaginary axis and the equilibria is stable and for the negative values of the *Det* both eigenvalues are on the real axis and the equilibria is unstable. Recall that a pitchfork bifurcation generically occurs when the determinant of the Jacobean matrix become zero [Strogatz, 2018]. Transforming (23) into the polar coordinate and substituting (18)-(20) in it yields the following expression for *Det* at the equilibrium points.

$$\text{For } R_1 \quad \text{Det} = 4\omega_n^2\omega_1^2 - 1 \quad (24)$$

$$\text{For } R_{2,3} \quad \text{Det} = +4(2\omega_n\omega_1 + 1) \quad (25)$$

$$\text{For } R_{4,5} \quad \text{Det} = -4(2\omega_n\omega_1 - 1) \quad (26)$$

The *Det* of the equilibrium points for different values of  $\omega_1$  are demonstrated in Fig. 1.

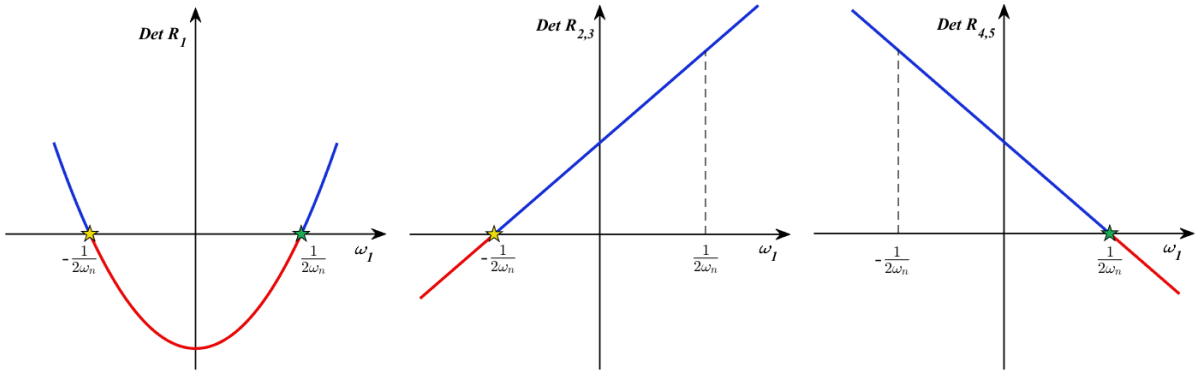


Fig. 1. Determinant at the equilibrium points around the first tongue

Besides, (19) and (20) provide the square value of the equilibrium points which impose a condition on the value of  $\omega_1$ . Therefore, existence of the real equilibria requires that for the case of hardening cubic nonlinearity ( $\alpha > 0$ ).

$$R_1 \quad \text{Exist} \quad \forall \quad \omega_1 \quad (27)$$

$$R_{2,3} \quad \text{Exist} \quad \forall \quad \omega_1 > -\frac{1}{2\omega_n} \quad (28)$$

$$R_{4,5} \quad \text{Exist} \quad \forall \quad \omega_1 > +\frac{1}{2\omega_n} \quad (29)$$

and for the case of softening cubic nonlinearity ( $\alpha < 0$ )

$$R_1 \quad \text{Exist} \quad \forall \quad \omega_1 \quad (30)$$

$$R_{2,3} \quad \text{Exist} \quad \forall \quad \omega_1 < -\frac{1}{2\omega_n} \quad (31)$$

$$R_{4,5} \quad \text{Exist} \quad \forall \quad \omega_1 < +\frac{1}{2\omega_n} \quad (32)$$

The corresponding bifurcation diagram for hardening and softening case is plotted in Fig. 2.

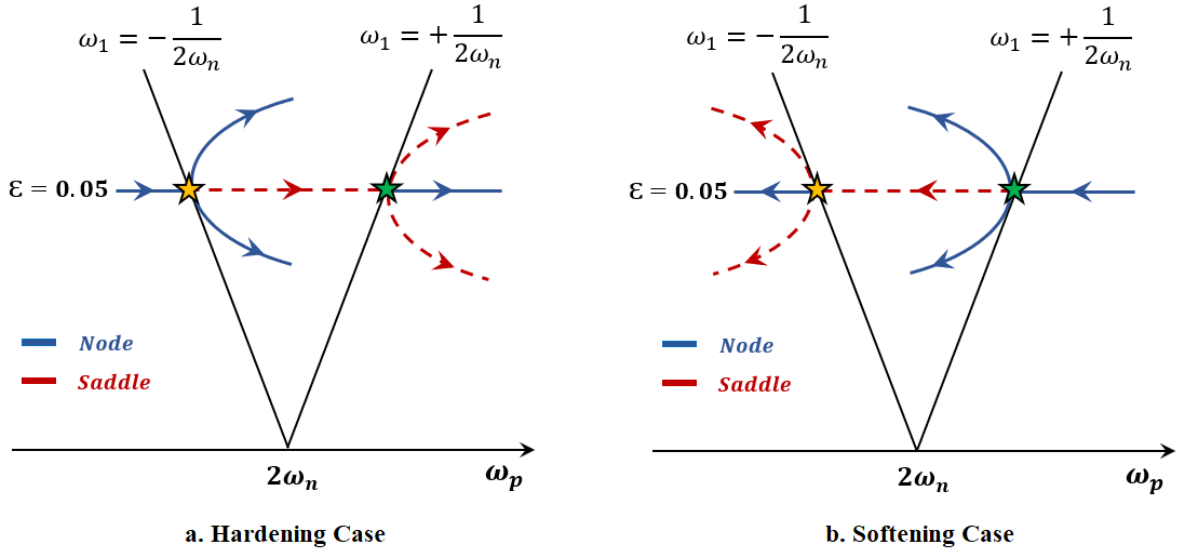


Fig. 2. Subcritical and supercritical pitchfork bifurcations around the first tongue

This analysis shows that for both hardening and softening nonlinearities, as one crosses the transition curves (for the constant value of  $\epsilon$ ) subcritical and supercritical pitchfork bifurcations (birth of new equilibria) occur. As illustrated in Fig. 2-a, for hardening nonlinearity, (27)-(29) requires that the origin is the only equilibria at the left-hand side of the first tongue. Meanwhile, Fig. 1 shows that by quasi statically increasing the value of  $\omega_1$  and approaching the left transition curve,  $Det$  of both  $R_1$  and  $R_{2,3}$  merge to zero. Consequently, by crossing the left transition curve  $Det$  of the Jacobian matrix at  $R_1$  and  $R_{2,3}$  cross  $\omega_1$  axis and a supercritical pitchfork bifurcation occurs, such that the equilibria at the origin becomes unstable and two new stable equilibria are born. Figure 1 shows that as  $\omega_1$  increase more and crosses the right transition curve,  $Det$  of Jacobian matrix at  $R_1$  and  $R_{4,5}$  cross the  $\omega_1$  axis and a subcritical pitchfork bifurcation occurs where the origin become stable again and two new unstable equilibria are born. Figure 2-b shows that the same sequence of events happens for the case of softening nonlinearity. The only difference is that (30)-(32) requires that origin is the only equilibria on the right-hand side of the first tongue and by quasi statically decreasing  $\omega_1$  and approaching the right transition curve,  $Det$  of  $R_1$  and  $R_{4,5}$  merge to zero and cause a supercritical pitchfork bifurcation. Greater decrease in the value of  $\omega_1$  causes a subcritical pitchfork bifurcation where the left transition curve is crossed and  $Det$  of  $R_1$  and  $R_{2,3}$  approach zero and cross the  $\omega_1$  axis.

## 2.2. Bifurcation Around the Second Tongue

To carry out this analysis for the second unstable tongue the general solution of (10) must be considered where

$$\omega_0 \neq 2\omega_n \quad (33)$$

In this case, removal of the secular terms requires

$$\left[ +\frac{3\alpha}{4\omega_0^2}(A^2 + B^2) - 2\left(\frac{\omega_1}{\omega_0}\right)\left(\frac{\omega_n}{\omega_0}\right)^2 \right] B = 0 \quad (34)$$

$$\left[ -\frac{3\alpha}{4\omega_0^2}(A^2 + B^2) + 2\left(\frac{\omega_1}{\omega_0}\right)\left(\frac{\omega_n}{\omega_0}\right)^2 \right] A = 0 \quad (35)$$

Removal of the resonant terms when  $\alpha = 0$  results in  $\omega_1 = 0$  for all the higher order tongue's transition curves. Besides, investigating the Jacobian matrix of (34) and (35) at corresponding equilibrium points

show that pitchfork bifurcation happens on the transition curves of the second tongue, where  $\omega_1$  become zero. But  $\omega_1 = 0$  is corresponded to both right and left transient curves. So it cannot predict what is happening within the second tongue and for more details on the stability change in this region higher orders of the perturbation analysis must be considered. By imposing (33) the general solution of (10) is obtained.

$$\begin{aligned}
 x_1(\tau) &= C \cos \frac{\omega_n}{\omega_0} \tau + D \sin \frac{\omega_n}{\omega_0} \tau \\
 &+ \frac{1}{2\omega_0(2\omega_n - \omega_0)} \left[ A \cos \left( \frac{\omega_n}{\omega_0} - 1 \right) \tau + B \sin \left( \frac{\omega_n}{\omega_0} - 1 \right) \tau \right] \\
 &+ \frac{1}{2\omega_0(2\omega_n + \omega_0)} \left[ A \cos \left( \frac{\omega_n}{\omega_0} + 1 \right) \tau + B \sin \left( \frac{\omega_n}{\omega_0} + 1 \right) \tau \right] \\
 &+ \frac{\alpha}{32\omega_n^2} \left[ (A^2 - 3B^2) A \cos \frac{3\omega_n}{\omega_0} \tau + (3A^2 - B^2) B \sin \frac{3\omega_n}{\omega_0} \tau \right]
 \end{aligned} \tag{36}$$

By inserting (9) and (36) in (8) and simplifying the trig functions one gets the following equation.

$$\begin{aligned}
x_2'' + \omega_0^2 x_2 = & \\
& \left[ 2 \left( \frac{\omega_2}{\omega_0} \right) \left( \frac{\omega_n}{\omega_0} \right)^2 + \left( \frac{\omega_1}{\omega_0} \right)^2 \left( \frac{\omega_n}{\omega_0} \right)^2 - \frac{1}{2\omega_0^2(\omega_0^2 - 4\omega_n^2)} - \frac{3\alpha^2}{128\omega_0^2\omega_n^2} (A^2 + B^2)^2 \right] \times \left[ A \cos \frac{\omega_n}{\omega_0} \tau + B \sin \frac{\omega_n}{\omega_0} \tau \right] \\
& - \frac{1}{\omega_0^3(\omega_0 - 2\omega_n)} \left[ \frac{3\alpha}{8} \frac{(3\omega_0 + 2\omega_n)}{(\omega_0 + 2\omega_n)} (A^2 + B^2) - \left( \frac{\omega_1}{\omega_0} \right) (\omega_0 - 2\omega_n)^2 \right] \times \left[ A \cos \left( \frac{\omega_n}{\omega_0} - 1 \right) \tau + B \sin \left( \frac{\omega_n}{\omega_0} - 1 \right) \tau \right] \\
& - \frac{1}{\omega_0^3(\omega_0 + 2\omega_n)} \left[ \frac{3\alpha}{8} \frac{(3\omega_0 - 2\omega_n)}{(\omega_0 - 2\omega_n)} (A^2 + B^2) - \left( \frac{\omega_1}{\omega_0} \right) (\omega_0 + 2\omega_n)^2 \right] \times \left[ A \cos \left( \frac{\omega_n}{\omega_0} + 1 \right) \tau + B \sin \left( \frac{\omega_n}{\omega_0} + 1 \right) \tau \right] \\
& - \frac{1}{4\omega_0^3(\omega_0 - 2\omega_n)} \left[ A \cos \left( \frac{\omega_n}{\omega_0} - 2 \right) \tau + B \sin \left( \frac{\omega_n}{\omega_0} - 2 \right) \tau \right] \\
& - \frac{1}{4\omega_0^3(\omega_0 + 2\omega_n)} \left[ A \cos \left( \frac{\omega_n}{\omega_0} + 2 \right) \tau + B \sin \left( \frac{\omega_n}{\omega_0} + 2 \right) \tau \right] \\
& - \frac{9\alpha}{16\omega_0^2} \left[ \frac{\alpha}{12\omega_n^2} (A^2 + B^2) - \frac{\omega_1}{\omega_0} \right] (A^2 - 3B^2) A \cos \frac{3\omega_n}{\omega_0} \tau \\
& - \frac{9\alpha}{16\omega_0^2} \left[ \frac{\alpha}{12\omega_n^2} (A^2 + B^2) - \frac{\omega_1}{\omega_0} \right] (3A^2 - B^2) B \sin \frac{3\omega_n}{\omega_0} \tau \\
& - \frac{\alpha}{8\omega_0^2} \left[ \frac{3}{\omega_0(\omega_0 - 2\omega_n)} + \frac{1}{8\omega_n^2} \right] (A^2 - 3B^2) A \cos \left( \frac{3\omega_n}{\omega_0} - 1 \right) \tau \\
& - \frac{\alpha}{8\omega_0^2} \left[ \frac{3}{\omega_0(\omega_0 - 2\omega_n)} + \frac{1}{8\omega_n^2} \right] (3A^2 - B^2) B \sin \left( \frac{3\omega_n}{\omega_0} - 1 \right) \tau \\
& - \frac{\alpha}{8\omega_0^2} \left[ \frac{3}{\omega_0(\omega_0 + 2\omega_n)} + \frac{1}{8\omega_n^2} \right] (A^2 - 3B^2) A \cos \left( \frac{3\omega_n}{\omega_0} + 1 \right) \tau \\
& - \frac{\alpha}{8\omega_0^2} \left[ \frac{3}{\omega_0(\omega_0 + 2\omega_n)} + \frac{1}{8\omega_n^2} \right] (3A^2 - B^2) B \sin \left( \frac{3\omega_n}{\omega_0} + 1 \right) \tau \\
& - \frac{3\alpha^2}{128\omega_0^2\omega_n^2} (A^4 - 10A^2B^2 + 5B^4) A \cos \frac{5\omega_n}{\omega_0} \tau \\
& - \frac{3\alpha^2}{128\omega_0^2\omega_n^2} (5A^4 - 10A^2B^2 + B^4) B \sin \frac{5\omega_n}{\omega_0} \tau \\
& - \left[ \left( \frac{3\alpha}{4\omega_0^2} (3A^2 + B^2) - 2 \left( \frac{\omega_1}{\omega_0} \right) \left( \frac{\omega_n}{\omega_0} \right)^2 \right) C + \frac{3\alpha}{4\omega_0^2} (2AB) D \right] \cos \frac{\omega_n}{\omega_0} \tau \\
& - \left[ \left( \frac{3\alpha}{4\omega_0^2} (A^2 + 3B^2) - 2 \left( \frac{\omega_1}{\omega_0} \right) \left( \frac{\omega_n}{\omega_0} \right)^2 \right) D + \frac{3\alpha}{4\omega_0^2} (2AB) C \right] \sin \frac{\omega_n}{\omega_0} \tau \\
& - \frac{1}{2\omega_0^2} \left[ C \cos \left( \frac{3\omega_n}{\omega_0} - 1 \right) \tau + D \sin \left( \frac{3\omega_n}{\omega_0} - 1 \right) \tau \right] \\
& - \frac{1}{2\omega_0^2} \left[ C \cos \left( \frac{3\omega_n}{\omega_0} + 1 \right) \tau + D \sin \left( \frac{3\omega_n}{\omega_0} + 1 \right) \tau \right] \\
& - \frac{3\alpha}{4\omega_0^2} \left[ (A^2 - B^2) C - (2AB) D \right] \cos \frac{3\omega_n}{\omega_0} \tau \\
& - \frac{3\alpha}{4\omega_0^2} \left[ (A^2 - B^2) D + (2AB) C \right] \sin \frac{3\omega_n}{\omega_0} \tau
\end{aligned} \tag{37}$$

which contains harmonic functions with frequencies equal to

$$\frac{\omega_n}{\omega_0}, \frac{\omega_n}{\omega_0} \pm 1, \frac{\omega_n}{\omega_0} \pm 2, \frac{3\omega_n}{\omega_0}, \frac{3\omega_n}{\omega_0} \pm 1, \frac{5\omega_n}{\omega_0} \tag{38}$$

The emanating frequency of the second tongue in the Ince-Strutt stability diagram is corresponded to the following special case [Nayfeh & Mook, 1995].

$$\left(\frac{\omega_n}{\omega_0}\right) - 2 = -\left(\frac{\omega_n}{\omega_0}\right) \rightarrow \omega_0 = \omega_n \quad (39)$$

which results in the following conditions for the elimination of the secular terms.

$$\begin{aligned} & \left[ +\frac{3\alpha^2}{128\omega_n^4}(A^2 + B^2)^2 - 2\left(\frac{\omega_2}{\omega_n}\right) - \left(\frac{\omega_1}{\omega_n}\right)^2 + \frac{1}{12\omega_n^4} \right] B + \\ & + \frac{3\alpha}{4\omega_n^2} [2AB]C + \left[ \frac{3\alpha}{4\omega_n^2}(A^2 + 3B^2) - 2\left(\frac{\omega_1}{\omega_n}\right) \right] D = 0 \end{aligned} \quad (40)$$

$$\begin{aligned} & \left[ -\frac{3\alpha^2}{128\omega_n^4}(A^2 + B^2)^2 + 2\left(\frac{\omega_2}{\omega_n}\right) + \left(\frac{\omega_1}{\omega_n}\right)^2 + \frac{5}{12\omega_n^4} \right] A + \\ & - \left[ \frac{3\alpha}{4\omega_n^2}(3A^2 + B^2) - 2\left(\frac{\omega_1}{\omega_n}\right) \right] C - \frac{3\alpha}{4\omega_n^2} [2AB]D = 0 \end{aligned} \quad (41)$$

Unlike the first tongue, where (13) and (14) contains only two variables ( $A$  and  $B$ ), (40) and (41) contains four variables ( $A, B, C$  and  $D$ ), which must be studied separately in ordered to investigate the stability and bifurcation around the second tongue. Collecting the multipliers of  $C$  and  $D$  results in the matrix form of (34) and (35) and does not provide any additional information. This is while, collecting the multipliers of  $A$  and  $B$  provides more details about the stability change within the second unstable tongue. In such a condition, removal of the resonant terms when  $\alpha = 0$  provides the second order multipliers of the second tongue's transition curves.

$$\omega_2 = -\frac{5}{24\omega_n^3}, +\frac{1}{24\omega_n^3} \quad (42)$$

By transforming the multipliers of  $A$  and  $B$  in (40) and (41) into polar coordinates

$$\left[ +\frac{3\alpha^2}{128\omega_n^4}R^4 - 2\left(\frac{\omega_2}{\omega_n}\right) - \left(\frac{\omega_1}{\omega_n}\right)^2 + \frac{1}{12\omega_n^4} \right] R \sin\theta = 0 \quad (43)$$

$$\left[ -\frac{3\alpha^2}{128\omega_n^4}R^4 + 2\left(\frac{\omega_2}{\omega_n}\right) + \left(\frac{\omega_1}{\omega_n}\right)^2 + \frac{5}{12\omega_n^4} \right] R \cos\theta = 0 \quad (44)$$

the following five equilibrium points are obtained.

$$R_1 = 0 \quad (45)$$

$$R_{2,3}^4 = \frac{128\omega_p^2}{3\alpha^2} \left( 2\left(\frac{\omega_2}{\omega_n}\right) + \left(\frac{\omega_1}{\omega_n}\right)^2 + \frac{5}{12\omega_p^2} \right) \quad \theta = 0, \pi \quad (46)$$

$$R_{4,5}^4 = \frac{128\omega_p^2}{3\alpha^2} \left( 2\left(\frac{\omega_2}{\omega_n}\right) + \left(\frac{\omega_1}{\omega_n}\right)^2 - \frac{1}{12\omega_p^2} \right) \quad \theta = \frac{\pi}{2}, \frac{3\pi}{2} \quad (47)$$

The local stability of these equilibrium points is determined by the eigenvalues of the Jacobian matrix corresponded to multipliers of  $A$  and  $B$  in (40) and (41).

$$J = \begin{bmatrix} \frac{3\alpha^2}{128\omega_n^4}(4AB)(A^2 + B^2) \\ -\frac{3\alpha^2}{128\omega_n^4}(A^4 + 6A^2B^2 + 5B^4) + 2\left(\frac{\omega_2}{\omega_n}\right) + \left(\frac{\omega_1}{\omega_n}\right)^2 \\ + \frac{3\alpha^2}{128\omega_n^4}(5A^4 + 6A^2B^2 + B^4) - 2\left(\frac{\omega_2}{\omega_n}\right) - \left(\frac{\omega_1}{\omega_n}\right)^2 \\ -\frac{3\alpha^2}{128\omega_n^4}(4AB)(A^2 + B^2) \end{bmatrix} \quad (48)$$

The *Tr* of (48) is always equal to zero and the value of the *Det* is expressed by the following equation.

$$\begin{aligned} Det(J) &= 5\left(\frac{3\alpha^2}{128\omega_n^4}\right)^2(A^2 + B^2)^4 \\ &- 6\left(\frac{3\alpha^2}{128\omega_n^4}\right)\left[\left(\frac{\omega_1}{\omega_n}\right)^2 + 2\left(\frac{\omega_2}{\omega_n}\right)\right](A^2 + B^2)^2 \\ &- \frac{2}{\omega_n^4}\left(\frac{3\alpha^2}{128\omega_n^4}\right)B^2(A^2 + B^2) \\ &+ \left[\left(\frac{\omega_1}{\omega_n}\right)^2 + 2\left(\frac{\omega_2}{\omega_n}\right) - \frac{1}{12\omega_n^4}\right]\left[\left(\frac{\omega_1}{\omega_n}\right)^2 + 2\left(\frac{\omega_2}{\omega_n}\right) + \frac{5}{12\omega_n^4}\right] \end{aligned} \quad (49)$$

Transforming (49) into polar coordinate and substituting (45)-(47) results in the following expressions for determinant at equilibrium points.

$$\text{For } R_1 \quad Det = \left[2\left(\frac{\omega_2}{\omega_n}\right) - \frac{1}{12\omega_n^4}\right]\left[2\left(\frac{\omega_2}{\omega_n}\right) + \frac{5}{12\omega_n^4}\right] \quad (50)$$

$$\text{For } R_{2,3} \quad Det = +\frac{2}{\omega_n^4}\left[2\left(\frac{\omega_2}{\omega_n}\right) + \frac{5}{12\omega_n^4}\right] \quad (51)$$

$$\text{For } R_{4,5} \quad Det = -\frac{2}{\omega_n^4}\left[2\left(\frac{\omega_2}{\omega_n}\right) - \frac{1}{12\omega_n^4}\right] \quad (52)$$

Figure 3 demonstrates *Det* at the equilibrium points for different values of  $\omega_2$ .

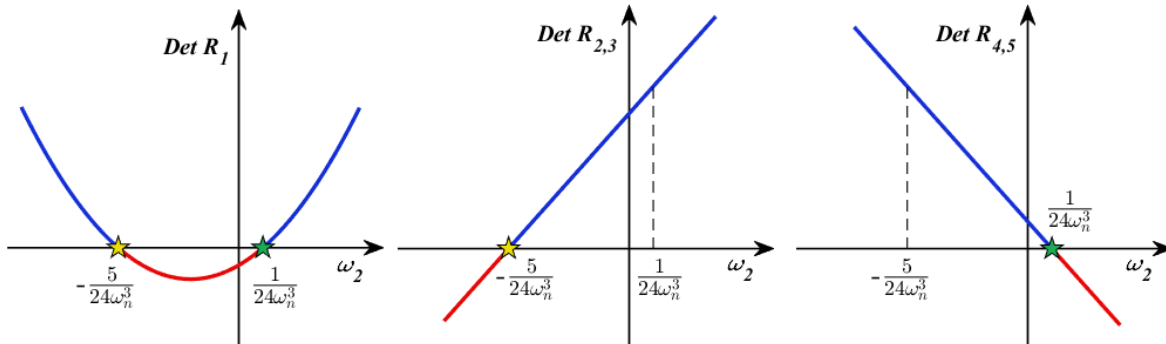


Fig. 3. Determinant at the equilibrium points around the second tongue

Besides, (46) and (47) provide the quad value of the equilibrium points which impose a condition on the value of  $\omega_2$ . Therefore, for the case of hardening cubic nonlinearity ( $\alpha > 0$ ) the existence of the real equilibria requires that

$$R_1 \quad \text{Exist} \quad \forall \quad \omega_2 \quad (53)$$

$$R_{2,3} \quad \text{Exist} \quad \forall \quad \omega_2 > -\frac{5}{24\omega_n^3} \quad (54)$$

$$R_{4,5} \quad \text{Exist} \quad \forall \quad \omega_2 > +\frac{1}{24\omega_n^3} \quad (55)$$

and for the case of softening cubic nonlinearity ( $\alpha < 0$ )

$$R_1 \quad \text{Exist} \quad \forall \quad \omega_2 \quad (56)$$

$$R_{2,3} \quad \text{Exist} \quad \forall \quad \omega_2 < -\frac{5}{24\omega_n^3} \quad (57)$$

$$R_{4,5} \quad \text{Exist} \quad \forall \quad \omega_2 < +\frac{1}{24\omega_n^3} \quad (58)$$

The corresponding bifurcation diagram for hardening and softening case is plotted in Fig. 4.

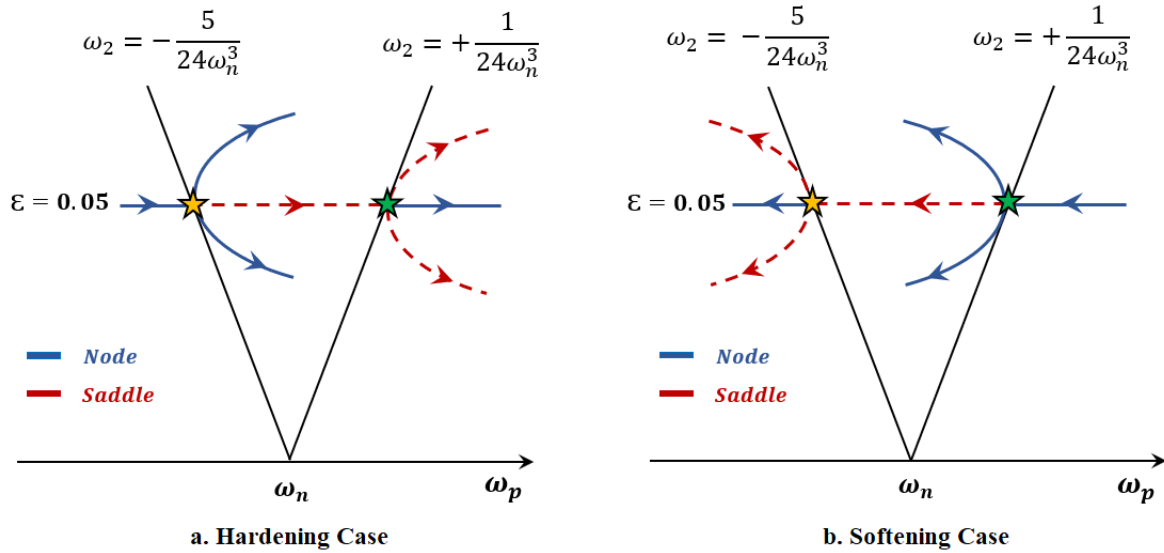


Fig. 4. Subcritical and supercritical pitchfork bifurcations around the second tongue

This analysis show that, as one crosses the transition curves of the second tongue (for the constant value of  $\epsilon$ ) the supercritical and subcritical pitchfork bifurcation occurs. Such that for the hardening nonlinearity, origin is the only equilibria at the left-hand side of the second tongue and by quasi statically increasing the value of the  $\omega_2$   $Det$  of the Jacobian matrix at  $R_1$  and  $R_{2,3}$  cross the  $\omega_2$  axis and results in a supercritical pitchfork bifurcation. Consequently, a subcritical pitchfork bifurcation happens when  $Det$  of the Jacobian matrix at  $R_1$  and  $R_{4,5}$  cross the  $\omega_2$  axis. Similarly, for the softening nonlinearity, the origin is the only equilibria at the right-hand side of the second tongue and by quasi statically decreasing  $\omega_2$ ,  $Det$  of  $R_1$  and  $R_{4,5}$  cross the  $\omega_2$  axis and cause a supercritical pitchfork bifurcation. Consequently, a subcritical pitchfork bifurcation happens when  $Det$  of Jacobian matrix at  $R_1$  and  $R_{2,3}$  cross the  $\omega_2$  axis.

### 2.3. Subharmonic Bifurcation

In this section the subharmonic bifurcation corresponded to the hardening case is investigated. Starting from (37) and choosing the following special condition from (38) [Nayfeh & Mook, 1995], provides the parametric frequency that the subharmonic bifurcation occurs.

$$\frac{3\omega_n}{\omega_0} - 1 = -\frac{\omega_n}{\omega_0} \rightarrow \omega_0 = 4\omega_n \quad (59)$$

Imposing (59) to (37) results in the following conditions for elimination of the secular terms.

$$\begin{aligned} & \left[ + \frac{3\alpha^2}{2048\omega_n^4}(A^2 + B^2)^2 - \frac{\alpha}{256\omega_n^4}(3A^2 - B^2) \right. \\ & \left. - \frac{1}{32} \left( \left( \frac{\omega_2}{\omega_n} \right) + \left( \frac{\omega_1}{\omega_n} \right)^2 + \frac{1}{12\omega_n^4} \right) \right] B + \frac{3\alpha}{4\omega_n^2} [2AB] C \\ & + \left[ \frac{3\alpha}{4\omega_n^2}(A^2 + 3B^2) - 2 \left( \frac{\omega_1}{\omega_n} \right) - \frac{1}{32\omega_n^2} \right] D = 0 \end{aligned} \quad (60)$$

$$\begin{aligned} & \left[ - \frac{3\alpha^2}{2048\omega_n^4}(A^2 + B^2)^2 - \frac{\alpha}{256\omega_n^4}(A^2 - 3B^2) \right. \\ & \left. + \frac{1}{32} \left( \left( \frac{\omega_2}{\omega_n} \right) + \left( \frac{\omega_1}{\omega_n} \right)^2 + \frac{1}{12\omega_n^4} \right) \right] A - \frac{3\alpha}{4\omega_n^2} [2AB] D \\ & - \left[ \frac{3\alpha}{4\omega_n^2}(3A^2 + B^2) - 2 \left( \frac{\omega_1}{\omega_n} \right) + \frac{1}{32\omega_n^2} \right] C = 0 \end{aligned} \quad (61)$$

As before, collecting the multipliers of  $C$  and  $D$  does not provide any additional information. But collecting the multipliers of  $A$  and  $B$  and transforming them into polar coordinates results in the following equations.

$$\begin{aligned} & \left[ + \frac{3\alpha^2}{2048\omega_n^4}R^4 - \frac{\alpha}{256\omega_n^4}R^2(2\cos 2\theta + 1) \right. \\ & \left. - \frac{1}{32} \left[ \left( \frac{\omega_2}{\omega_n} \right) + \left( \frac{\omega_1}{\omega_n} \right)^2 + \frac{1}{12\omega_n^4} \right] R \sin \theta \right] = 0 \end{aligned} \quad (62)$$

$$\begin{aligned} & \left[ - \frac{3\alpha^2}{2048\omega_n^4}R^4 - \frac{\alpha}{256\omega_n^4}R^2(2\cos 2\theta - 1) \right. \\ & \left. + \frac{1}{32} \left[ \left( \frac{\omega_2}{\omega_n} \right) + \left( \frac{\omega_1}{\omega_n} \right)^2 + \frac{1}{12\omega_n^4} \right] R \cos \theta \right] = 0 \end{aligned} \quad (63)$$

Solving (62) and (63) results in the following nine equilibrium points.

$$R_1 = 0 \quad (64)$$

$$\begin{aligned} R_{2,3,4,5}^2 &= \frac{4}{3\alpha} \left( -1 + \sqrt{\frac{3}{2}\omega_1^2\omega_n^2 + 12\omega_2\omega_n^3} \right) \\ & , \theta = 0, \frac{\pi}{2}, \pi, \frac{3\pi}{2} \end{aligned} \quad (65)$$

$$\begin{aligned} R_{6,7,8,9}^2 &= \frac{4}{3\alpha} \left( +1 + \sqrt{\frac{3}{2}\omega_1^2\omega_n^2 + 12\omega_2\omega_n^3} \right) \\ & , \theta = \frac{\pi}{4}, \frac{3\pi}{4}, \frac{5\pi}{4}, \frac{7\pi}{4} \end{aligned} \quad (66)$$

The local stability of these equilibrium points is determined by the eigenvalues of the Jacobian matrix corresponded to multipliers of  $A$  and  $B$  in (60) and (61).

$$J = \begin{bmatrix} \frac{3\alpha^2}{2048\omega_n^4}(4AB)(A^2 + B^2) - \frac{3\alpha}{256\omega_n^4}(2AB) \\ -\frac{3\alpha^2}{2048\omega_n^4}(5A^4 + 6A^2B^2 + B^4) - \frac{3\alpha}{256\omega_n^4}(A^2 - B^2) - \frac{1}{32}\left(\left(\frac{\omega_2}{\omega_n}\right) + \left(\frac{\omega_1}{\omega_n}\right)^2 + \frac{1}{12\omega_n^4}\right) \\ \frac{3\alpha^2}{2048\omega_n^4}(A^4 + 6A^2B^2 + 5B^4) - \frac{3\alpha}{256\omega_n^4}(A^2 - B^2) + \frac{1}{32}\left(\left(\frac{\omega_2}{\omega_n}\right) + \left(\frac{\omega_1}{\omega_n}\right)^2 + \frac{1}{12\omega_n^4}\right) \\ -\frac{3\alpha^2}{2048\omega_n^4}(4AB)(A^2 + B^2) + \frac{3\alpha}{256\omega_n^4}(2AB) \end{bmatrix} \quad (67)$$

The  $Tr$  of (67) is always equal to zero and the value of the  $Det$  is expressed by the following equation.

$$\begin{aligned} Det(J) &= 5 \left( \frac{3\alpha^2}{2048\omega_n^4} \right)^2 (A^2 + B^2)^4 \\ &- 4 \left( \frac{3\alpha}{256\omega_n^4} \right) \left( \frac{3\alpha^2}{2048\omega_n^4} \right) (A^2 + B^2) \left( (A^2 - B^2) - 4A^2B^2 \right) \\ &- \frac{3}{16} \left( \left( \frac{\omega_2}{\omega_n} \right) + \frac{1}{8} \left( \frac{\omega_1}{\omega_n} \right)^2 + \frac{5}{12\omega_n^4} \right) \left( \frac{3\alpha^2}{2048\omega_n^4} \right) (A^2 + B^2)^2 \\ &+ \frac{1}{1024} \left( \left( \frac{\omega_2}{\omega_n} \right) + \left( \frac{\omega_1}{\omega_n} \right)^2 + \frac{1}{12\omega_n^4} \right)^2 \end{aligned} \quad (68)$$

By transforming (68) into the polar coordinate and substituting (64)-(66) the following expressions are obtained for the determinant at the equilibrium points.

$$\text{For } R_1, Det = \frac{1}{1024} \left( \left( \frac{\omega_2}{\omega_n} \right) + \left( \frac{\omega_1}{\omega_n} \right)^2 + \frac{1}{12\omega_n^4} \right)^2 \quad (69)$$

$$\begin{aligned} \text{For } R_{2,3,4,5} Det &= \frac{1}{3072\omega_n^8} \left[ 2(\omega_1^2\omega_n^2 + 8\omega_2\omega_n^3) \right. \\ &\left. - (\omega_1^2\omega_n^2 + 8\omega_2\omega_n^3 + \frac{2}{3}) + \sqrt{\frac{3}{2}\omega_1^2\omega_n^2 + 12\omega_2\omega_n^3} \right] \end{aligned} \quad (70)$$

$$\begin{aligned} \text{For } R_{6,7,8,9} Det &= \frac{1}{3072\omega_n^8} \left[ 2(\omega_1^2\omega_n^2 + 8\omega_2\omega_n^3) \right. \\ &\left. + (\omega_1^2\omega_n^2 + 8\omega_2\omega_n^3 + \frac{2}{3}) + \sqrt{\frac{3}{2}\omega_1^2\omega_n^2 + 12\omega_2\omega_n^3} \right] \end{aligned} \quad (71)$$

Figure 5 demonstrates  $Det$  at the equilibrium points for different values of  $\omega_2$ .

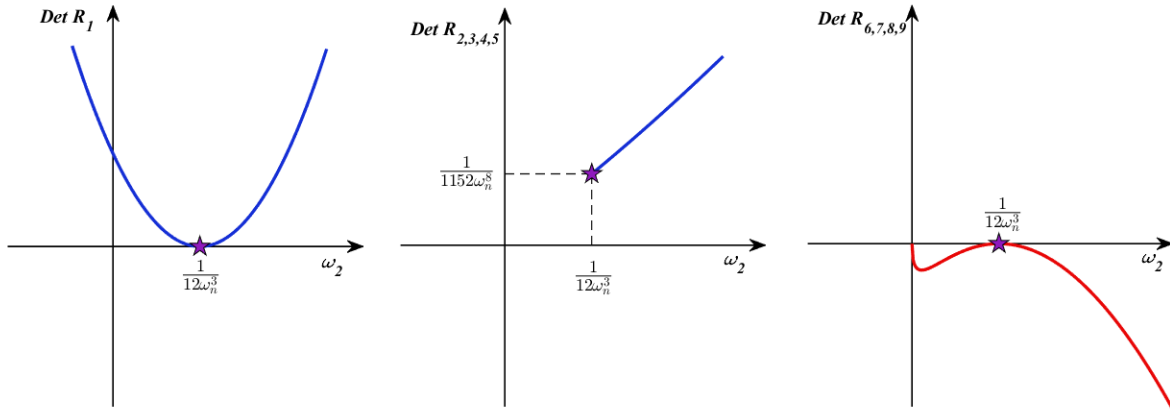


Fig. 5. Determinant at equilibrium points for relatively large values of parametric frequency

Besides, (65) and (66) provide the square value of the equilibrium points which impose a condition on the value of  $\omega_2$ . Therefore, for the case of hardening ( $\alpha > 0$ ) the existence of the real equilibria requires that

$$R_1 \quad \text{Exist} \quad \forall \quad \omega_2 \quad (72)$$

$$R_{2,3,4,5} \quad \text{Exist} \quad \forall \quad \omega_2 > \frac{1}{12\omega_n^3} \quad (73)$$

$$R_{6,7,8,9} \quad \text{Exist} \quad \forall \quad \omega_2 > 0 \quad (74)$$

The corresponding bifurcation diagram is plotted in Fig. 6.

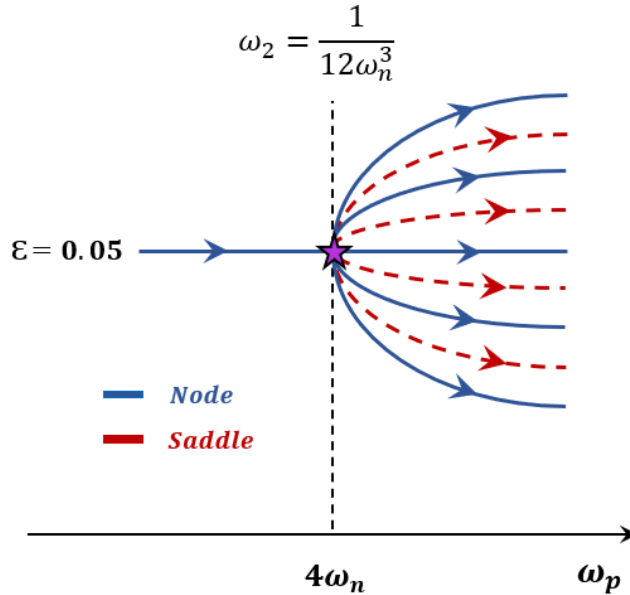


Fig. 6. Subharmonic bifurcation for small values of undamped natural frequency

This analysis shows that by quasi statically increasing the value of  $\omega_2$  (for constant value of  $\epsilon$ ) the subharmonic bifurcation occurs when  $Det$  of  $R_1$ , the trivial equilibria at origin, becomes zero. Figure 5 shows that, unlike the pitchfork bifurcations occurring around the unstable tongues, in the subharmonic bifurcation the stability of the equilibria at origin does not change, as  $Det$  of  $R_1$  becomes zero but it does not

cross the  $\omega_2$  axis and remains positive afterward. Figure 5 show that after  $Det$  of  $R_1$  becomes zero,  $Det$  of the Jacobian matrix at  $R_{2,3,4,5}$  and  $R_{6,7,8,9}$  has positive and negative values, which is corresponded to the newly-born stable and unstable nontrivial equilibria, respectively. Finally, Figs. 7 and 8 demonstrate the global bifurcation diagram of the hardening and softening nonlinear cases, respectively.

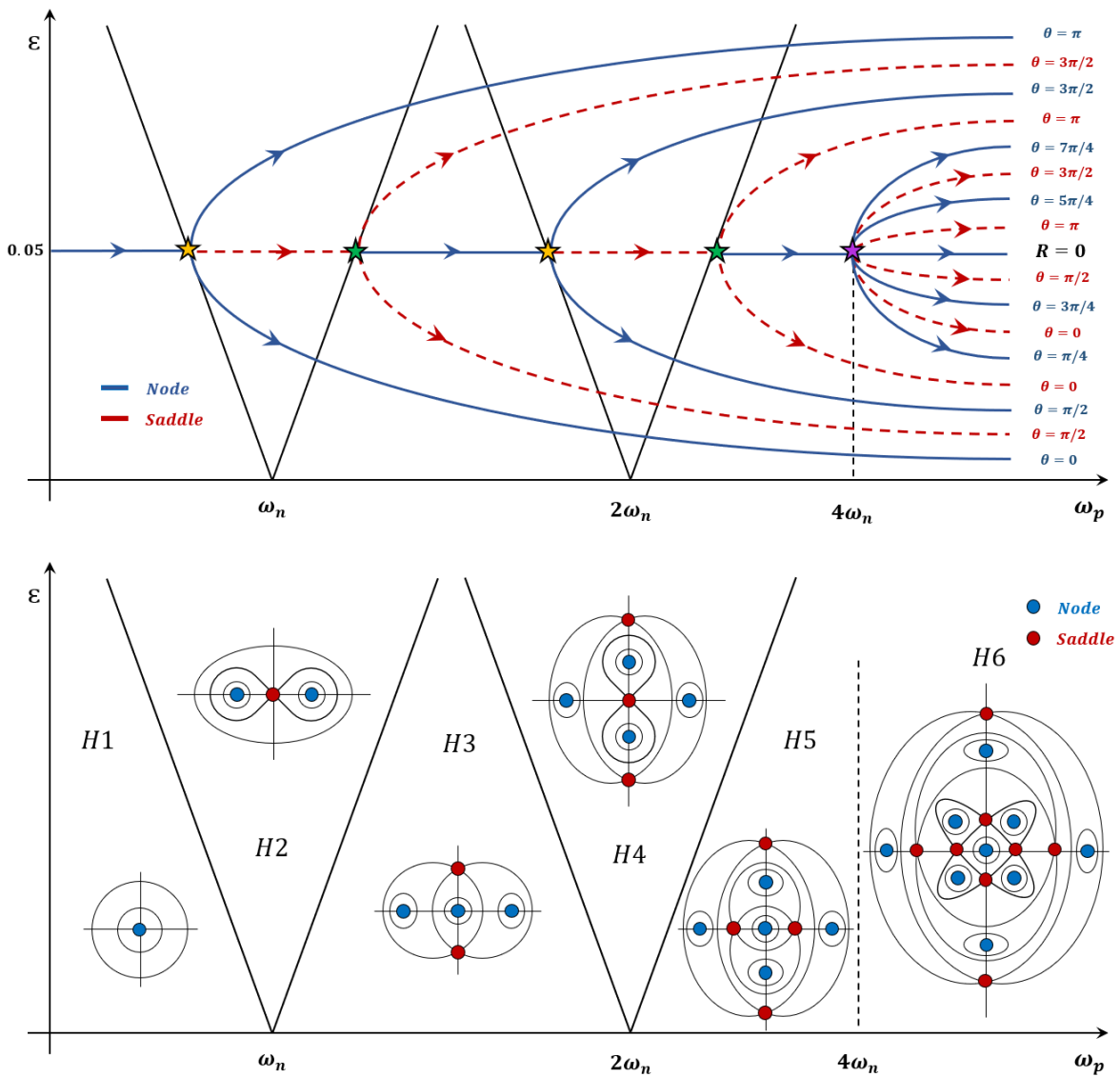


Fig. 7. Overall bifurcation diagram for the Mathieu equation with hardening nonlinear term

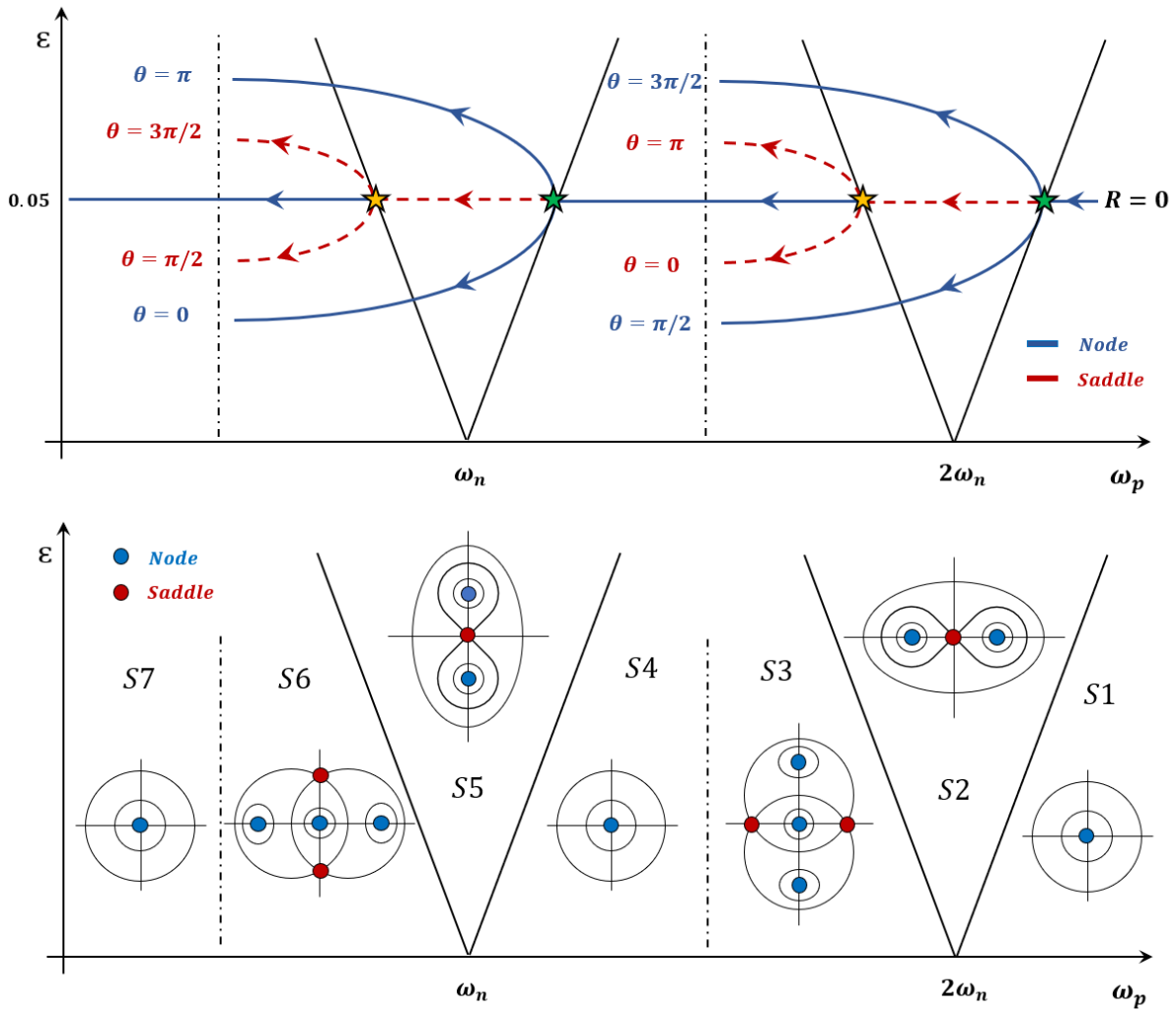


Fig. 8. Overall bifurcation diagram for the Mathieu equation with softening nonlinear term

### 3. Numerical Simulation

In this section, the foregoing analytical analysis is compared with the results obtained from numerical integration which is completed in MATLAB using Runge-Kutta of the fourth-fifth order.

#### 3.1. Poincare Map

Figures 9-17 exhibit the Poincare map of the Mathieu equation with hardening nonlinear term and Figs. 18-24 exhibit the Poincare map of the softening nonlinearity, all corresponding to the surface of section at  $t = \omega_p/2\pi$ . In these plots, a stable equilibrium point (node) appear in shape of a O and an unstable equilibrium point (saddle) appear in shapes of a X. For both hardening and softening cases the origin is always a node outside the instability regions, and a saddle inside the instability regions. Figure 9 is corresponded to  $H1$  region in Fig. 7, indicating that there is only one stable equilibria (node) in this region.

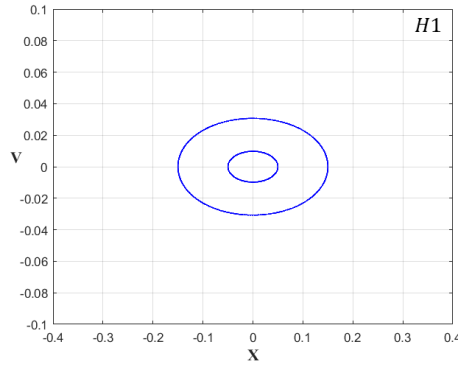


Fig. 9. Poincaré map portraits of the hardening case, for  $F_p = 0.05, \omega_n = 0.20, \omega_p = 0.4$

Figure 10 show that by crossing the left-hand side transition curve of the second tongue, this node turns into a saddle and two nodes are born on the horizontal axis.

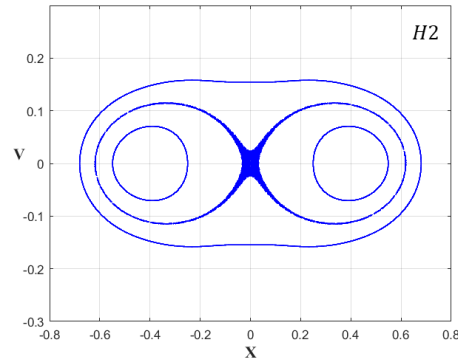


Fig. 10. Poincaré map portraits of the hardening case, for  $F_p = 0.05, \omega_n = 0.25, \omega_p = 0.25$

Consequently, by crossing the right-hand side transition curve of the second tongue the origin turns into a node again and two saddles are born on the vertical axis. The already existing nontrivial nodes remain intact while they move away from the origin.

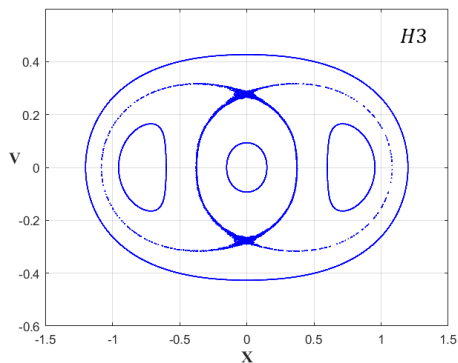


Fig. 11. Poincaré map portraits of the hardening case, for  $F_p = 0.05, \omega_n = 0.25, \omega_p = 0.3$

Figure 12 shows that, by crossing the left-hand side transition curve of the first tongue, the origin turns into a saddle again and another two nodes are born on the vertical axis, while the other nontrivial equilibria

do not change and move further from the origin.



Fig. 12. Poincaré map portraits of the hardening case, for  $F_p = 0.05, \omega_n = 0.25, \omega_p = 0.5$

Finally, by crossing the right-hand side transition curve of the first tongue the origin becomes a node and two saddles are born on the horizontal axis

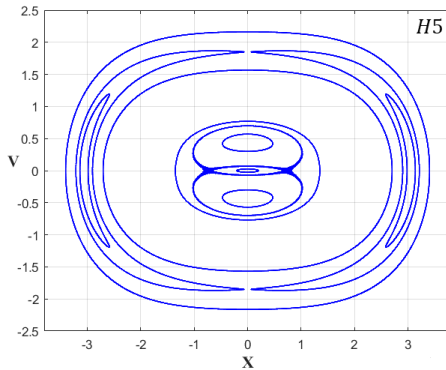


Fig. 13. Poincaré map portraits of the hardening case, for  $F_p = 0.05, \omega_n = 0.25, \omega_p = 0.65$

At this point, by increasing the parametric frequency several subharmonic bifurcations take place. Figures 14-17 show the first four subharmonic bifurcations, such that equal numbers of nodes and saddles are borne simultaneously. As the number of nodes and saddles, which are born around the origin, are equal, the stability of the origin does not change. Only the subharmonic bifurcation occurring in Fig. 17 was predicted by the analytical calculations which is corresponded to H6 region in Fig. 7. Prediction of the subharmonic bifurcation demonstrated in Figs. 14-16 requires higher order perturbation analysis. Figures 9-13 show that the radius of the nontrivial equilibria grows in amplitude rapidly by increasing the parametric frequency and creation of the new equilibria. This is while, Figs. 14-17 show that the occurrence of the subharmonic bifurcations does not significantly change the location of already existing nontrivial equilibria.

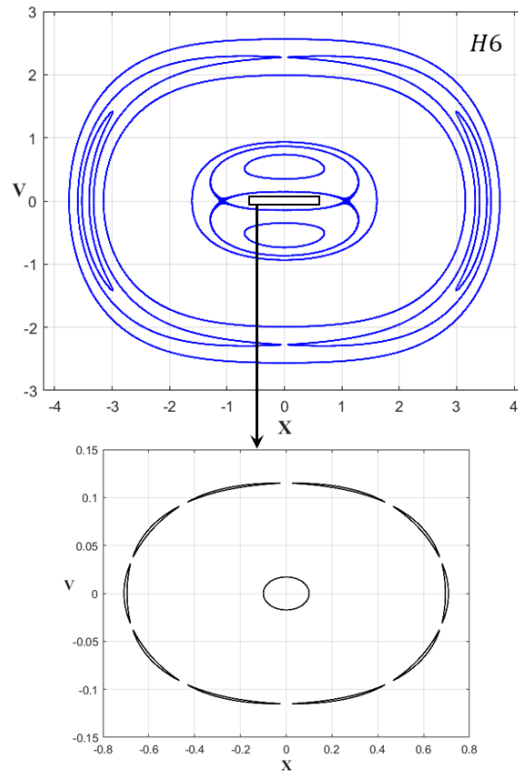


Fig. 14. Poincaré map portraits of the hardening case, for  $F_p = 0.05, \omega_n = 0.25, \omega_p = 0.72$

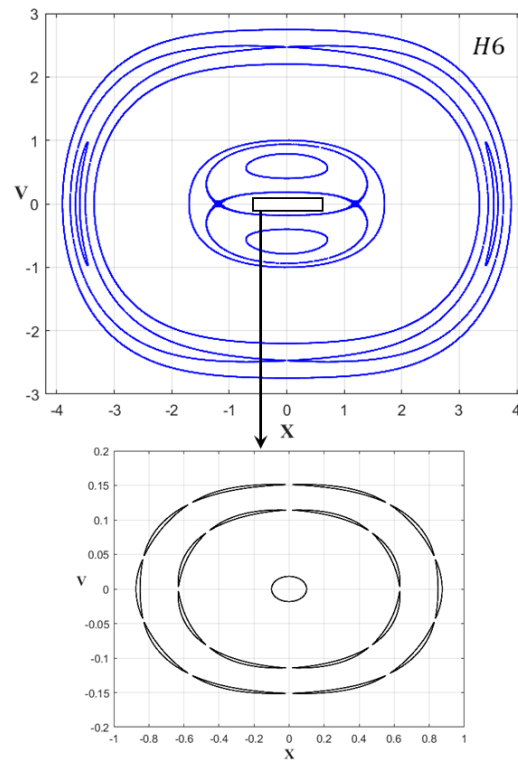


Fig. 15. Poincaré map portraits of the hardening case, for  $F_p = 0.05, \omega_n = 0.25, \omega_p = 0.75$

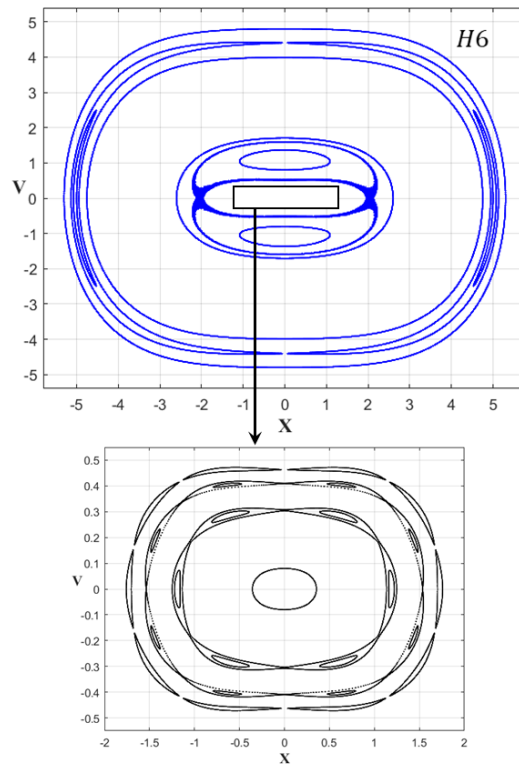


Fig. 16. Poincaré map portraits of the hardening case, for  $F_p = 0.05, \omega_n = 0.25, \omega_p = 1$

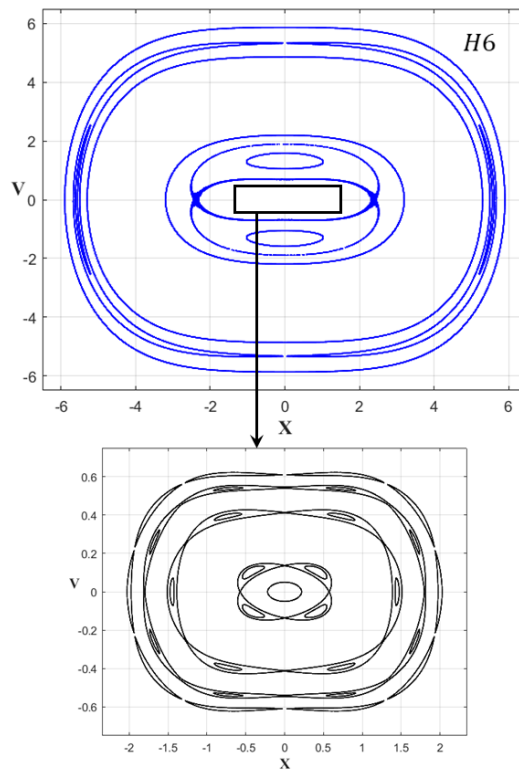


Fig. 17. Poincaré map portraits of the hardening case, for  $F_p = 0.05, \omega_n = 0.25, \omega_p = 1.1$

The same sequence of events happens for the Mathieu equation with softening nonlinear term. As demonstrated in Fig. 18, there is only one node at origin within  $S1$  region of Fig. 8 and by decreasing the parametric frequency and crossing the transition curves, the stability of the equilibrium point at origin changes and more nodes and saddles are borne on the horizontal and vertical axes. The only difference is that, by decreasing the parametric frequency, the nontrivial equilibria move more distant from the origin and fall into the unstable region, which is a characteristic of the softening nonlinear case and it can be observed in  $S3$  and  $S4$  regions as well as in  $S6$  and  $S7$  regions of Fig. 8.

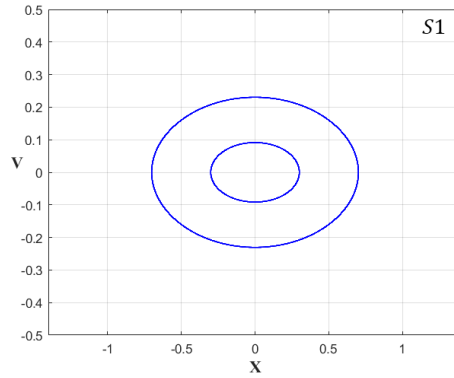


Fig. 18. Poincaré map portraits of the softening case, for  $F_p = 0.05, \omega_n = 0.5, \omega_p = 1.1$

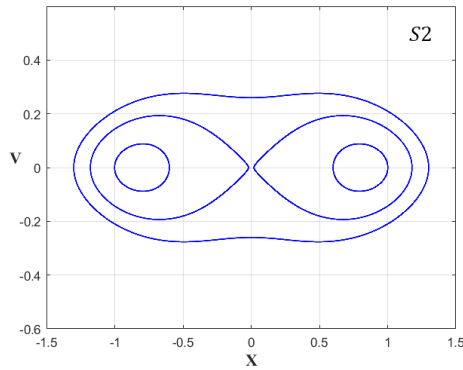


Fig. 19. Poincaré map portraits of the softening case, for  $F_p = 0.05, \omega_n = 0.5, \omega_p = 1$

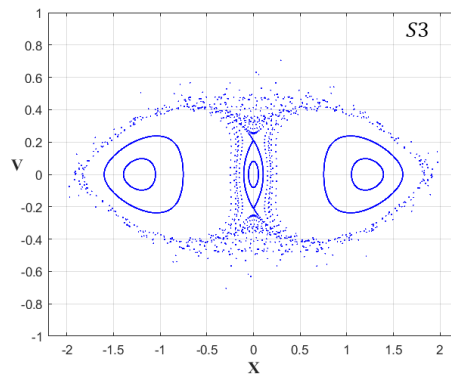


Fig. 20. Poincaré map portraits of the softening case, for  $F_p = 0.05, \omega_n = 0.5, \omega_p = 0.935$

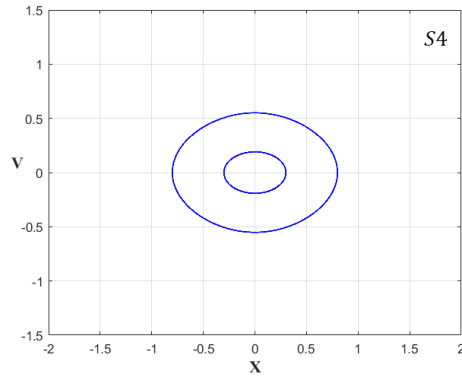


Fig. 21. Poincaré map portraits of the softening case, for  $F_p = 0.05, \omega_n = 0.5, \omega_p = 0.75$

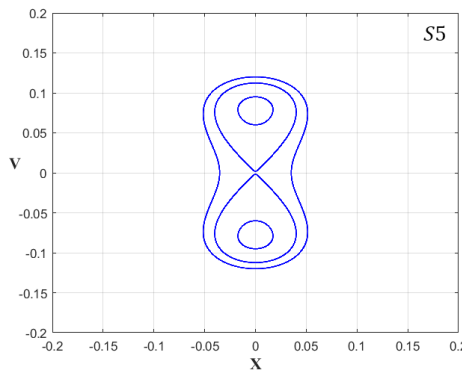


Fig. 22. Poincaré map portraits of the softening case, for  $F_p = 0.05, \omega_n = 0.5, \omega_p = 0.5$

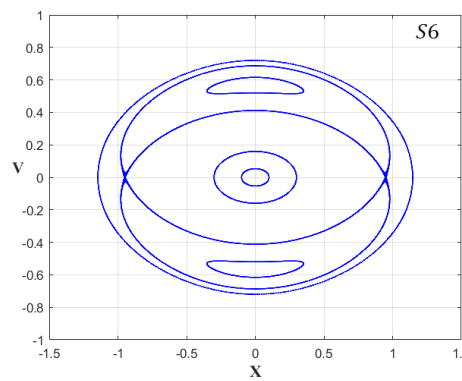


Fig. 23. Poincaré map portraits of the softening case, for  $F_p = 0.05, \omega_n = 0.5, \omega_p = 0.45$

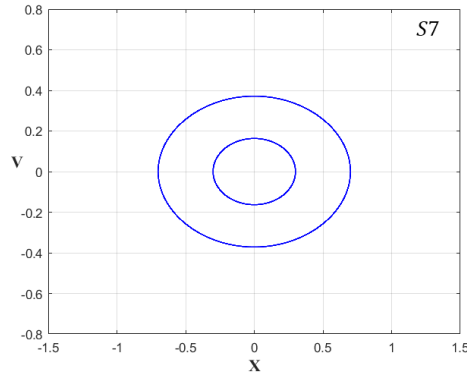


Fig. 24. Poincaré map portraits of the softening case, for  $F_p = 0.05, \omega_n = 0.5, \omega_p = 0.4$

### 3.2. Phase Plane

Figures 25 and 26 demonstrate the phase plane of the hardening and softening cases for different parametric frequencies while the rest of the parameters are kept constant. For all the plots the integration starts from the initial condition of  $x(0) = [0.1 \ 0]$ , specified by red dot in the plots, and for duration of  $100T$ , where  $T$  is the period of the parametric frequency. Considering that the value of the undamped natural frequency is  $\omega_n = 1$ , the phase planes corresponded to  $\omega_p = 2$  and  $\omega_p = 1$  represents system response within the first and second unstable tongues respectively,  $\omega_p = 1.5$  and  $\omega_p = 0.5$  represent system response outside and on the left-hand side of the first and second unstable tongues, respectively, and finally  $\omega_p = 4.5$  and  $\omega_p = 3.5$  represent system response after and before occurrence of the subharmonic bifurcation, respectively.

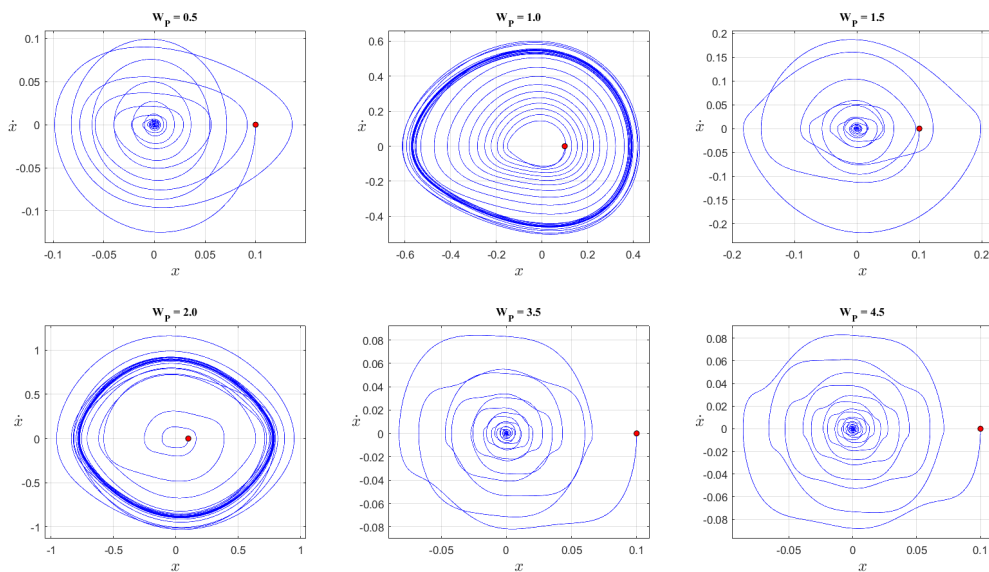


Fig. 25. Phase plane for the hardening case,  $\zeta = 0.08, \omega_n = 1, \alpha = +0.75, F_p = 0.75,$

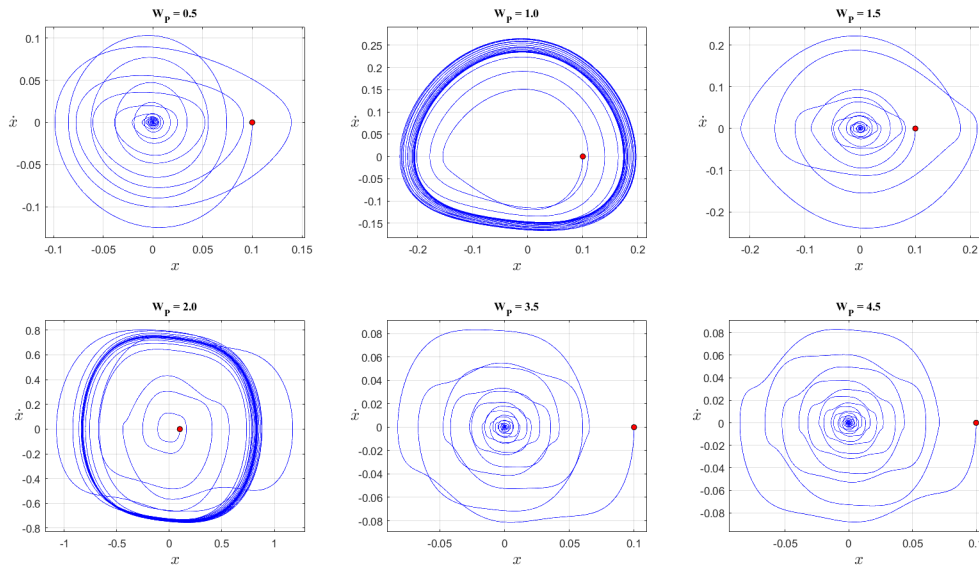


Fig. 26. Phase plane for the softening case,  $\zeta = 0.08$ ,  $\omega_n = 1$ ,  $\alpha = -0.75$ ,  $F_p = 0.75$ ,

#### 4. Conclusion

In this work, Poincaré-Lindstedt method is used to study both pitchfork and subharmonic bifurcations of the Mathieu-Duffing equation at the same time, such that the results can be demonstrated in the parameter space of parametric frequency. The corresponding global bifurcation diagram is provided for both hardening and softening cases. These diagrams show that for the hardening nonlinearity, by crossing the transition curves of the first and second tongues two saddles are born on the vertical and horizontal axes, respectively, while for the softening nonlinearity the newborn saddles are on the horizontal and vertical axes, respectively. Both analytical and numerical results show that the change of the stability and creation of the new equilibria occur only at the equilibria at origin and not at the nontrivial equilibrium points. The numerical results show that by occurrence of the supercritical and subcritical pitchfork bifurcations around the unstable tongues, the location of the nontrivial equilibrium points changes significantly, while the occurrence of the subharmonic bifurcations at the location of the nontrivial equilibrium points does not change notably. Numerical studies show that there are several subharmonic bifurcations occurring for relatively large values of the parametric frequency, but none of these subharmonic bifurcations change the stability of the origin, as an equal number of stable and unstable equilibrium points are born simultaneously. Finally, the saddle shaped nature of the origin inside the unstable tongues justifies the amplitude detuning effect of the nonlinear equation rather than an unbounded response of the linear case within the unstable tongue.

#### References

- Acar, G. & Feeny, B. F. [2016] “Floquet-based analysis of general responses of the mathieu equation,” *Journal of Vibration and Acoustics* **138**, doi:10.1115/1.4033341, URL <https://doi.org/10.1115/1.4033341>.
- Cveticanin, L. & Kovacic, I. [2007] “Parametrically excited vibrations of an oscillator with strong cubic negative nonlinearity,” *Journal of Sound and Vibration* **304**, 201–212, doi:10.1016/j.jsv.2007.02.028, URL <https://doi.org/10.1016/j.jsv.2007.02.028>.
- Jazar, R. N., Mahinfalah, M., Mahmoudian, N. & Rastgaar, M. A. [2008] “Energy-rate method and stability chart of parametric vibrating systems,” *Journal of the Brazilian Society of Mechanical Sciences and Engineering* **30**, 182–188, doi:10.1590/s1678-58782008000300002, URL <https://doi.org/10.1590/s1678-58782008000300002>.
- Kovacic, I., Rand, R. & Sah, S. M. [2018] “Mathieu's equation and its generalizations: overview of stability

- charts and their features,” *Applied Mechanics Reviews* **70**, doi:10.1115/1.4039144, URL <https://doi.org/10.1115/1.4039144>.
- Leung, A. Y. T., Guo, Z. & Yang, H. X. [2012] “Transition curves and bifurcations of a class of fractional mathieu-type equations,” *International Journal of Bifurcation and Chaos* **22**, 1250275, doi:10.1142/s0218127412502756, URL <https://doi.org/10.1142/s0218127412502756>.
- Morrison, T. M. & Rand, R. H. [2007] “2:1 resonance in the delayed nonlinear mathieu equation,” *Nonlinear Dynamics* **50**, 341–352, doi:10.1007/s11071-006-9162-5, URL <https://doi.org/10.1007/s11071-006-9162-5>.
- Nayfeh, A. H. & Mook, D. T. [1995] *Nonlinear oscillations* (Wiley), doi:10.1002/9783527617586, URL <https://doi.org/10.1002/9783527617586>.
- Ng, L. & Rand, R. [2002] “Bifurcations in a mathieu equation with cubic nonlinearities: Part II,” *Design Engineering* (ASMEDC), doi:10.1115/imece2002-32410, URL <https://doi.org/10.1115/imece2002-32410>.
- Ramakrishnan, V. & Feeny, B. F. [2012] “Resonances of a forced mathieu equation with reference to wind turbine blades,” *Journal of Vibration and Acoustics* **134**, doi:10.1115/1.4006183, URL <https://doi.org/10.1115/1.4006183>.
- Rand, R. & Morrison, T. [2005] “2:1:1 resonance in the quasi-periodic mathieu equation,” *Nonlinear Dynamics* **40**, 195–203, doi:10.1007/s11071-005-6005-8, URL <https://doi.org/10.1007/s11071-005-6005-8>.
- Rodriguez, A. & Collado, J. [2015] “On stability of periodic solutions in non-homogeneous hill's equation,” *2015 12th International Conference on Electrical Engineering, Computing Science and Automatic Control (CCE)* (IEEE), doi:10.1109/iceee.2015.7357958, URL <https://doi.org/10.1109/iceee.2015.7357958>.
- Shivamoggi, B. K. [2003] *Perturbation methods for differential equations* (Birkhäuser Boston), doi:10.1007/978-1-4612-0047-5, URL <https://doi.org/10.1007/978-1-4612-0047-5>.
- Strogatz, S. H. [2018] *Nonlinear Dynamics and Chaos* (CRC Press), doi:10.1201/9780429492563, URL <https://doi.org/10.1201/9780429492563>.
- Subhadip, B. & K., B. J. [2019] “On the properties of a class of higher-order mathieu equations originating from a parametric quantum oscillator,” *Nonlinear Dynamics* **96**, 737–750, doi:10.1007/s11071-019-04818-9, URL <https://doi.org/10.1007/s11071-019-04818-9>.
- Welte, J., Kniffka, T. J. & Ecker, H. [2013] “Parametric excitation in a two degree of freedom MEMS system,” *Shock and Vibration* **20**, 1113–1124, doi:10.1155/2013/502109, URL <https://doi.org/10.1155/2013/502109>.
- Zounes, R. S. & Rand, R. H. [2002] “Subharmonic resonance in the non-linear mathieu equation,” *International Journal of Non-Linear Mechanics* **37**, 43–73, doi:10.1016/s0020-7462(00)00095-0, URL [https://doi.org/10.1016/s0020-7462\(00\)00095-0](https://doi.org/10.1016/s0020-7462(00)00095-0).